Catal Lett (2009) 127:323–333
DOI 10.1007/s10562-008-9683-2

High Efficient Production of Hydrogen from Bio-oil Using Low-temperature Electrochemical Catalytic Reforming Approach Over NiCuZn–Al_2O_3 Catalyst

Tongqi Ye · Lixia Yuan · Yaqiong Chen · Tao Kan · Jing Tu · Xifeng Zhu · Youshifumi Torimoto · Mitsuo Yamamoto · Quanxin Li

Received: 10 July 2008 / Accepted: 18 September 2008 / Published online: 11 November 2008

Abstract High-efficient production of hydrogen from bio-oil was performed by a novel electrochemical catalytic reforming method over the NiCuZn–Al_2O_3 catalyst. The influences of current on the hydrogen yield, carbon conversion and products' distribution were investigated. Both the hydrogen yield and carbon conversion were remarkably enhanced by the current through the catalyst, reaching nearly complete conversion with a hydrogen yield of 93.5% even at low reforming temperature of 400 °C. The thermal electrons would play important roles in promoting the reforming reactions of the oxygenated-organic compounds in bio-oil, molecular dissociation and the catalyst reduction.

Keywords Hydrogen · Bio-oil · NiCuZn–Al_2O_3 Catalyst · Electrochemical catalytic reforming

1 Introduction

Hydrogen is considered to be clean fuel and could have an important role in reducing environmental emissions for the future. Especially, its production is an attractive subject of current interest for fuel cell applications [1–3], which are considered to have the potential to provide a clean energy source for automobile as an alternative to gasoline or diesel engines. Most of the present world energy demand comes from fossil fuels [1–3]. Unlike fossil fuels, hydrogen burns cleanly, without emitting any environmental pollutants. In addition, hydrogen also possesses the highest energy content per unit of weight (about 120.7 MJ/kg), compared to any of the known fuels. Hydrogen is also an important raw material for the chemical industry, which is mainly used for ammonia production, followed by refining and methanol production etc. Currently, hydrogen commercially-used is primarily produced from methane, and other hydrocarbon feedstocks such as naphtha, heavy residues from petrochemical processes, coke oven gas, and coal are also used for production of hydrogen [2, 4]. Electrolysis, in some place, has also been used to produce hydrogen [2]. The use of lignocellulosic biomass as a new feedstock for hydrogen production or energy source has attracted considerable attention in recent years [3, 5–9], because it is not only be environmentally friendly but also would open new opportunities for utilization of renewable resources, which are globally available.

Bio-oil, generated mainly from biomass via fast pyrolysis process [10–17], generally contains numerous and complex oxygenated organic compounds including acids, alcohols, aldehydes, ketones, substituted phenolics and other oxygenates derived from biomass carbohydrates and lignin [18]. Bio-oil represents another potential source of renewable chemicals [10, 12, 19]. The route of the steam reforming of bio-oil involves fast pyrolysis of biomass to generate bio-oil, and reforming of it to produce a gaseous rich-hydrogen mixture. Probably, production hydrogen from bio-oil reforming is one of the most promising options

T. Ye · L. Yuan · Y. Chen · T. Kan · J. Tu · X. Zhu · Q. Li (✉)
Department of Chemical Physics, Lab of Biomass Clean Energy, University of Science & Technology of China, Hefei, Anhui 230026, People's Republic of China
e-mail: liqx@ustc.edu.cn

Y. Torimoto
Oxy Japan Corporation, 7# Floor, Miya Building, 4-3-4, Kojimachi, Chiyoda-ku, Tokyo 102-0083, Japan

M. Yamamoto
College of Arts and Sciences, The University of Tokyo, 3-8-1 Komaba, Meguro-ku 153-8902, Japan

because it can achieve high hydrogen yield and high content of hydrogen. The steam reforming of the bio-oil would be mainly determined by the ability of a catalyst to catalyze the steam reforming reactions of the oxygenated organic compounds ($C_nH_mO_k$) in bio-oil ($C_nH_mO_k + (n - k)$ $H_2O = nCO + (n + m/2 - k)$ H_2), the water-shift reaction ($CO + H_2O \rightarrow CO_2 + H_2$). In the case of the high temperature reforming of bio-oil, partial thermal decomposition of bio-oil and the Boudouard reaction ($2CO = CO_2 + C$) may simultaneously occur [20–22]. Various catalysts have been selected and used for production of hydrogen via the steam reforming of hydrocarbons [23, 24]. Conventional steam reforming catalysts for the steam reforming of hydrocarbons are 10–33 wt.% NiO on a mineral support (e.g., alumina, magnesia) [25, 26], usually operating at $T = 600$–700 °C and $S/C = 5$–13. More recently, it has been revealed that the Ni–Cu bimetallic catalysts supported on SiO_2, Al_2O_3, ZnO/Al_2O_3 exhibited acceptable activity, stability and selectivity to hydrogen from low-temperature ethanol steam reforming and ethanol oxidative steam reforming [27–33]. In the above systems, Cu is the active agent and promotes fast ethanol dehydrogenation to acetaldehyde, Ni promotes C–C bond rupture of acetaldehyde to produce CH_4 and CO and increases hydrogen selectivity. For the catalytic steam reforming of the bio-oil [20, 25, 34–41], ethanol [1, 2, 22, 28–31, 33, 42–45], or other model oxygenates (e.g., acetic acid, ethylene glycol) [46–57], it has been widely explored via the reforming catalysts including the oxide catalysts, the Ni-based catalysts, and noble metal-loaded catalysts etc. Lower reforming temperature is essential from the viewpoint of economy. Noble metals (Pt, Ru, Rh) are generally more effective than the Ni-based catalysts and less carbon depositing [58–61]. Such catalysts are not common in real applications because of their high cost. Another hindering for the catalytic reforming of bio-oil is the deactivation of catalysts due to coke or oligomer deposition even in the presence of an excess of steam ($S/_C > 5$) [26, 50]. Thus, it is very significant to realize low temperature reforming of bio-oil using non-noble metal catalysts. It is also important to decrease carbon deposits during the bio-oil reforming process.

In our previous work, attention has been paid to the fast pyrolysis of biomass [13–17] and the production of hydrogen and bio-syngas from bio-oil [39–42] and the synthesis of liquid bio-fuels such as gasoline and diesel etc. [40]. We have investigated the catalytic steam reforming for bio-oil and ethanol by using the reforming catalysts of Ni/Al_2O_3, C12A7–O^-, C12A7–O^-/MgO, C12A7–O^-/CeO, MgO/Al_2O_3, Pt/Al_2O_3 [39–42]. In particular, the catalyst's activity of the C12A7 ($12CaO \cdot 7Al_2O_3$) and metal-doped ones have been investigated for the bio-oil's reforming [39] and oxidation of the organic compounds [39]. Moreover, the Fischer-Tropsch synthesis (FTS) by using the bio-syngas, derived from the bio-oil reforming, has also been investigated as a potential approach to obtaining clean liquid bio-fuels [40]. In this work, an electrified Ni–Cr wire was used for heating the catalyst and synchronously providing the thermal electrons onto the catalyst during the bio-oil reforming, described as the electrochemical catalytic reforming (ECR) mode. The idea of the ECR approach rooted in the study of the anionic emission materials in our previous work, in which the diffusion of thermal electrons on the oxide material surface and the dissociation of the small molecules on the surface were identified [62, 63]. Here, the effects of current on the bio-oil reforming and the microcosmic properties of the NiCuZn–Al_2O_3 catalyst were studied. The mechanism of the electrochemical catalytic reforming for bio-oil was also discussed based on present investigations.

2 Experimental

2.1 Catalyst Preparation and Characterization

The NiCuZn–Al_2O_3 reforming catalysts with settled Cu:Ni:Zn ratio were prepared by the co-precipitation method at a constant pH (9.0 ± 0.3) using respective metal nitrates as precursors and a mixture of NaOH (1 M) and Na_2CO_3 (1 M) as precipitants. The precipitate was washed to pH = 7 and then dried overnight in an oven at 110 °C, then heated at 1 °C/min in air to 450 °C and calcined at 450 °C for 5 h to obtain the corresponding mixed oxide catalysts. All samples were reduced in situ before use in a hydrogen flow at 350 °C for 1 h.

The metallic element contents in the prepared catalysts were measured by inductively coupled plasma and atomic emission spectroscopy (ICP/AES, Atom scan Advantage of Thermo Jarrell Ash Corporation, USA). According to the ICP/AES, a trace amount of sodium element was observed in the prepared catalysts (about 0.26 wt.%). The Brunauer-Emmett-Teller (BET) surface area and pore volume was determined by the N_2 physisorption at −196 °C using a COULTER SA 3100 analyzer. The surface elements and their states were analyzed by X-ray photoelectron spectroscopy (XPS,). The XPS measurements were performed on an ESCALAB-250 (Thermo-VG Scientific, USA) spectrometer with Al Ka (1486.6 eV) irradiation source. The normalized XPS intensities, which are proportional to the concentrations of the corresponding elements in the surface layer, were determined as the integrated peak area divided by their corresponding sensitivity factor. The C(1*s*) peak at 284.6 eV was generally used as a calibration standard for determining the peaks' position and the elemental concentration. The X-ray diffraction (XRD) was

measured on an X'pert Pro Philips diffractometer with a Cu Kα radiation.

2.2 Bio-oil

Bio-oil, produced by the fast pyrolysis of biomass in a circulating fluidized bed with a capacity of 120 kg/h of oil at our Lab (patent: ZL01263584.7). Temperature for the biomass pyrolysis generally ranged from 520 to 540 °C, which was supplied by the byproducts of charcoal formed in the bio-oil production process. The pyrolysis of biomass was generally performed with a heating rate of about 10^4 °C/s for a residence time of less than 2 s and was followed by a fast cooling process. The main products of the fast pyrolysis of biomass consisted of liquid bio-oil (55–70 wt.%), a mixture gaseous products (e.g., CO_2, CO, CH_4, etc.), and charcoal. The bio-oil produced is a dark-brown organic liquid and comprise different molecular weight products, derived from depolymerization and fragmentation reactions of three key biomass building blocks: cellulose, hemicellulose, and lignin. Therefore, the elemental composition of bio-oil varied with different feedstocks of biomass. Some physical and chemical properties of the bio-oils derived from the sawdust, rice husk, and cotton stalk powder were summarized in Table 1. The bio-oils contain a large number of complex compounds such as hydroxyaldehydes, hydroxyketones, sugars, carboxylic acids, phenolics, and so forth. The distribution of these compounds depends on the type of biomass used and on the pyrolysis process conditions (temperature, residence time, and heating rate). Because the main elemental composition of the pyrolysis bio-oils was C, H, and O (Table 2), the oxygenated organic compounds in the pyrolysis bio-oils were generally described by a chemical formula of $C_nH_mO_k \cdot xH_2O$. For the bio-oil derived from sawdust, the chemical formula is $CH_{1.48}O_{0.53} \cdot 0.32H_2O$. The crude biomass pyrolysis oil also contain some amounts of nonvolatile materials (35–40 wt.%), such as sugars and oligomeric phenolics etc., which are generally difficult to be reformed. Particularly, these nonvolatile materials easily form carbon depositions on the catalyst surface and lead to the fast deactivation of catalysts when the crude oil was directly fed into the reforming reactor. Thus, in this work, the volatile organic components of the crude bio-oil derived from the sawdust, pretreated by vapor the crude bio-oil from 80 °C to 180 °C, were used for the reforming experiments. The amount of the volatile organic components was about 50–60 wt.% of the crude oil. Table 2 shows some chemical properties of crude bio-oil and the pretreated bio-oil derived from the sawdust. The oxygenated organic compound in the volatile components was represented as a chemical formula of $CH_{2.03}O_{0.67} \cdot 0.89H_2O$. For the reforming of the heavy part of the bio-oil, we are going to use dual tube reactors and on-line recover the inactive catalyst in the production process of hydrogen. Moreover, the residuals after the pretreatment would be used as a fuel for combustion.

Table 2 Some chemical properties for the crude and pretreated bio-oils derived from the sawdust

Composition (wt.%)	Crude bio-oil	Pretreated bio-oil
H_2O	21.0	39.3
	Elemental composition (wt.%)	
C	54.5	48.5
H	6.7	8.2
O	38.7	43.3
Chemical formula	$CH_{1.48}O_{0.53} \cdot 0.32H_2O$	$CH_{2.03}O_{0.67} \cdot 0.89H_2O$

2.3 Reaction System

As shown in Fig. 1, the bio-oil steam reforming experiments were carried out in the continuous flow systems, using a quartz fixed-bed reactor under atmospheric pressure. To obtain a stable and quantitative carbon-feeding, the bio-oil was fed into the reactors using the micro-injection pumps (Model: TS2-60, Longer Precision Pump). On the other hand, the steam from the steam-generator was simultaneously fed into the reactors for adjusting the *S/C* ratio (mol ratio of steam to carbon in bio-oil fed). The steam amount fed and the effluent gases from the reactors were controlled and measured by the mass flow controllers. The steam amount was also calibrated before running the reforming experiments. Temperature and its' distribution were measured by the thermocouples inserted into the catalyst beds. We performed and compared with the bio-oil reforming experiments with following two modes, i.e., the common catalytic reforming (CSR) mode and the

Table 1 The elemental compositions and characteristics of bio-oils derived from the sawdust, rice husk, and cotton stalk powder

Feedstocks	Elements in bio-oil (wt.%)			H_2O (wt.%)	Ash (wt.%)	Density (kg/m^3)	LHV (MJ/kg)	PH
	C	H	O					
Sawdust	54.5	6.7	38.7	21.0	0.07	1,300	18.20	2.1
Rice husk	41.0	7.4	51.2	24.5	0.08	1,150	17.16	3.2
Cotton stalk	42.3	7.9	49.4	24.4	0.07	1,160	17.77	3.3

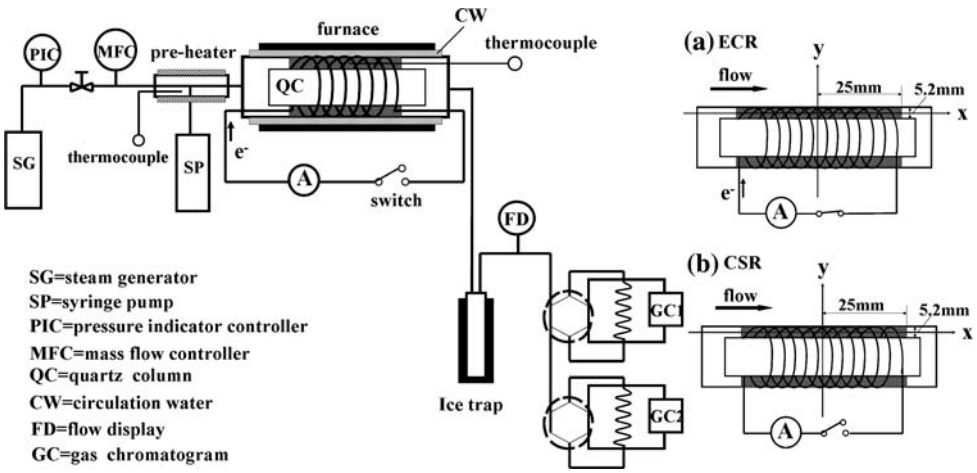

Fig. 1 Schematic setup of the fixed-bed flow reaction system for the bio-oil (left). Right: **a** ECR mode: the catalyst was uniformly embedded around the Ni–Cr wire, which passed through an ac electronic current for heating the catalyst and synchronously providing the electrons onto the catalyst. **b** CSR mode: the current was shut off and the reactor was homogeneously heated by an outside furnace

electrochemical catalytic reforming (ECR) mode. For CSR mode (Fig. 1b), a given amount of powder catalyst of NiCuZn–Al_2O_3 was installed in the middle zone of the reactor, and homogeneously heated by an outside furnace. The power source applied to the Ni–Cr wire was shut off (Fig. 1b). In the case of the ECR mode (Fig. 1a), an annular Ni–Cr wire which was used for heating the catalyst and providing the electrons onto the catalyst, was installed in the reactor. The catalyst was uniformly embedded around the Ni–Cr wire, which passed through a given ac electronic current. To make a certain reforming temperature, the catalyst bed was heated supplementarily by an outside furnace or cooled via a circulation-water system.

Temperature distributions in the catalyst bed under different conditions were first measured by the thermocouples inserted into different position in the bed. As shown in Table 3, the flow speed of the mixture gas and the heating modes (i.e., ECR and CSR) mainly affected the temperature distribution in the catalyst bed. When temperature in the center of the ECR catalyst bed was near 550 °C, the maximal temperature gradients in the transverse orientation and in the longitudinal orientation for low flow speed condition (total flow: 30 mL/min) were about 13 °C and 24 °C respectively. With increasing the flow speed, maximal temperature gradients both in the transverse and longitudinal orientation increased, reaching about 17 °C and 32 °C respectively for total flow speed of 300 mL/min. On the other hand, the temperature gradients for the CSR mode are smaller than those in the ECR mode. In practice, the temperature distribution in the catalyst bed was tested before running the reforming experiments. The relationship between the averaged temperature in the catalyst bed (T_{average}) and the center temperature ($T_{(0,\ 0)}$) was obtained form the temperature distribution measured under different experimental conditions. Thus, the averaged temperature needed can be adjusted by the center temperature through the power applied to the Ni–Cr wire and/or the outside oven. Moreover, the temperature in the center of the catalyst bed, generally, is close to the average temperature (the deviations between the center temperature and the average value in the bed were less than 10 °C) in our investigated range (400–600 °C). Here, the averaged temperature in the catalyst bed was approximately used as the reaction temperature in the ECR or CSR experiments.

The products of the bio-oil steam reforming reactions were analyzed by two on-line gas chromatographs (GC1 and GC2) with thermal conductivity detector (TCD). Ultra-high purity argon (99.999%) was used as carrier gas. The products of H_2, CO and CH_4 and other hydrocarbons were detected by GC1 (Molecular Sieve 5A). The CO_2 formed was detected by GC2 (GDX-502). The composition of the effluent gases from the reactor was also confirmed by a Q-MS mass spectrometer (Mode: GSD 300 Omnistar). The reforming performance of the bio-oil was studied by measuring the hydrogen yield, carbon conversion and dry gas composition under different reforming conditions. The hydrogen yield was calculated as a percentage of the stoichiometric potential, considering a complete conversion of carbon element in the bio-oil to CO_2 according to the reaction ($C_nH_mO_k + (2n - k)\ H_2O = (2n + m/2 - k)\ H_2 + nCO_2$) [20, 35]. The potential yield of hydrogen is $(2n + m/2 - k)$ mole per mole of carbon in the feed. The carbon conversion was calculated by total mol carbon in the gaseous products divided by the mol carbon in the fed bio-oil (i.e., the ratio of the mol carbon in the effluent gases to the carbon in the bio-oil fed). The carbon balance was defined as the ratio of all carbon-containing product moles (including coke) to the consumed moles of the oxygenated organic compounds ($C_nH_mO_k$), accounting for stoichiometry. Generally, all experiments were repeated three times. The difference for each repeating, in general, ranged from zero to about 10%.

The intermediates desorbed from the catalyst surface were mass analyzed by a time-of-flight (TOF) mass spectrometer at a background vacuum of about 1×10^{-4} Pa. The experimental setup of the TOF system has been

Table 3 Typical temperature distribution in the catalyst bed for the CSR and ECR modes at 1 atm

Modes	f_{total} (mL/min)	I_{inside} (A)	Position[a]	T (°C)	$T_{averaged}$ (°C)
CSR	0	0	(0, 0)	552	
			(25 mm, 0)	551	
			(−25 mm, 0)	550	
			(0, 1.5 mm)	553	
			(0, −1.5 mm)	551	
					551.4
CSR	30	0	(0, 0)	550	
			(25 mm, 0)	556	
			(−25 mm, 0)	547	
			(0, 1.5 mm)	553	
			(0, −1.5 mm)	549	
					551.0
CSR	300	0	(0, 0)	549	
			(25 mm, 0)	555	
			(−25 mm, 0)	543	
			(0, 1.5 mm)	552	
			(0, −1.5 mm)	547	
					549.2
ECR	0	3	(0, 0)	552	
			(25 mm, 0)	548	
			(−25 mm, 0)	548	
			(0, 1.5 mm)	544	
			(0, −1.5 mm)	562	
					550.8
ECR	30	3	(0, 0)	551	
			(25 mm, 0)	555	
			(−25 mm, 0)	542	
			(0, 1.5 mm)	540	
			(0, −1.5 mm)	564	
					550.4
ECR	300	3	(0, 0)	553	
			(25 mm, 0)	558	
			(−25 mm, 0)	541	
			(0, 1.5 mm)	537	
			(0, −1.5 mm)	569	
					551.6

[a] The coordinate in the CSR bed and in the ECR catalyst bed were shown in Fig. 1 (b) and (a). The coordinate (0, 0) stands for the center of the bed

described in detail elsewhere [64]. Here, a quartz-tube reactor was installed in the center of the sample chamber of the TOF system. The reactants or carrier gas (argon) were fed onto the quartz-tube reactor by a nozzle with a total pressure of about 10^{-1} Pa in the reactor tube. A small amount of the products (including intermediates formed in the reforming reactions) passed through a pinhole of about 100 μm locating in the center of the quartz-tube reactor, which allows a simultaneous analysis via the TOF mass spectrometry.

3 Results and Discussion

It was observed that addition of copper to the Ni-based catalysts significantly promoted the reforming activity for the bio-oil in the lower temperature region. The NiCuZn–Al_2O_3 catalyst with an optimal Ni:Cu:Zn molar ratio near 2.5:1.0:1.2 was used in this study based on the screening tests of the catalyst. The Brunauer-Emmett-Teller (BET) surface area and pore volume was about 212.3 m^2/g and 0.48 cm^3/g. The performance of the bio-oil's reforming using the conventional steam reforming method, generally, mainly controlled by the reforming temperature for a given catalyst. In this work, it was observed interestingly that the behavior of the bio-oil's reforming was very sensitive to the current (I) through the NiCuZn–Al_2O_3 catalyst, which was described as the electrochemical catalytic reforming. To investigate the features of the bio-oil's electrochemical catalytic reforming, we performed the bio-oil's reforming under different current, meanwhile other experimental conditions (i.e., T (temperature), *S/C* (the ratio of stream to carbon fed), and *GHSV* (gas hourly space velocity)) were maintained.

Figure 2 shows dependence of the carbon conversion and the hydrogen yield on the current (I) under the different fixed reforming temperature (T = 300 °C, 350 °C, 400 °C, 450 °C, 500 °C, 550 °C, and 600 °C, respectively, $S/C = 6.3$; $GHSV = 5{,}200\ h^{-1}$). In the case of $I = 0$ (i.e., the conventional reforming mode), the carbon conversion was only 9.6% at 300 °C. On the current through the NiCuZn–Al_2O_3 catalyst (i.e., the electrochemical catalytic reforming model), however, the carbon conversion was remarkably enhanced by the current, particularly at lower temperature (300–400 °C). The carbon conversion increased from 9.6% to 88.3% with increasing the current from 0 to 4 A at 300 °C, and reaches 97.5% at 4 A and 400 °C. On the other hand, the hydrogen yield also increased with increasing the current at various fixed reforming temperature. For the common catalytic reforming (i.e., $I = 0$ A) over the NiCuZn–Al_2O_3 catalyst, the hydrogen yield was very low (about 2.5%) at $T = 300$ °C, $S/C = 6.3$, and $GHSV = 5{,}200\ h^{-1}$. With increasing the current to 4 A, however, the hydrogen yield remarkably increased to 86.2% at the same low temperature of 300 °C. The above results indicate that the hydrogen production from the bio-oil low-temperature reforming can be realized by the electrochemical catalytic reforming approach and using the NiCuZn–Al_2O_3 reforming catalyst. It has been revealed that the production of hydrogen from bio-oil via the conventional stream reforming method over the Ni–Al_2O_3 catalyst usually should operate at higher temperature [26].

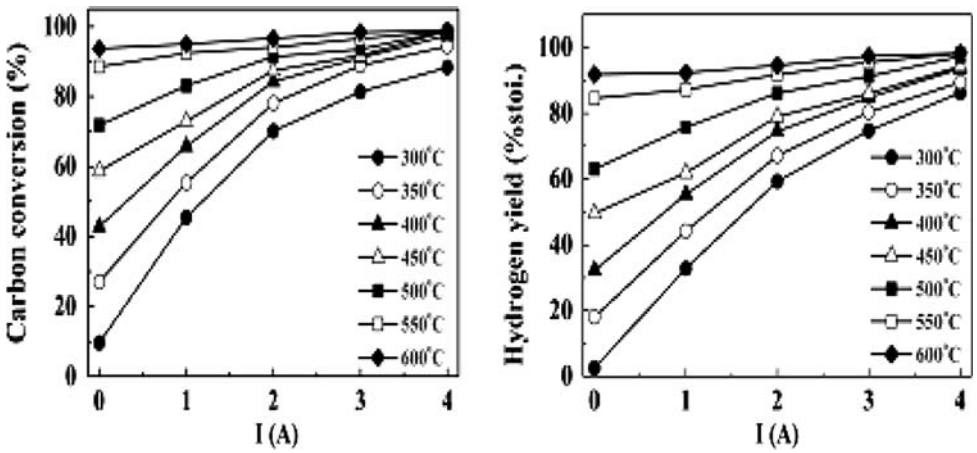

Fig. 2 Effect of the current on the carbon conversion (left) and the hydrogen yield (right), measured as a function of current through the NiCuZn–Al_2O_3 catalyst at different fixed temperature. Reforming conditions: $T = 300$ °C, 350 °C, 400 °C, 450 °C, 500 °C, 550 °C and 600 °C respectively, $S/C = 6.3$, $GHSV = 5{,}200\ h^{-1}$, and $P = 1$ atm

For example, the carbon conversion and the yield of hydrogen can reach over 90% by the conventional reforming method, but higher reforming temperature (over 700 °C) is required [26, 42]. Alternatively, it is possible to produce hydrogen from bio-oil with high carbon conversion (>90%) and hydrogen yield (>90%) at low-reforming temperature (over 350 °C) by using the electrochemical catalytic reforming over the NiCuZn–Al_2O_3 catalyst.

Figure 3 depicts the influence of the current on the composition of the gaseous products over the NiCuZn–Al_2O_3 catalyst (reforming conditions: $I = 0$–4 A, $T = 450$ °C, $S/C = 6.3$, $GHSV = 5{,}200\ h^{-1}$, and $P = 1$ atm). Hydrogen is the major product (66–70 vol.%) together with smaller amount by-products of CO_2 (27–30 vol.%) and CO (1–3 vol.%). A trace amount of CH_4 (<1.5 vol.%) and/or C_2H_4 (<0.3 vol.%) was also observed in the effluent carbonaceous compounds. It was found that the concentration of CO slightly increased with increasing the current, accompanied by the concentration decrease of CO_2, CH_4, and C_2H_4. In particular, the distributions of the un-reformed by-products of CH_4 and C_2H_4 are near zero at higher current. The composition of the products from the reforming of the bio-oil includes the gaseous products, the liquid products and the solid products (e.g., coke). In order to further quantitatively study the reforming product distribution, we evaluated the carbon balance in the ECR and CSR processes of the bio-oil. Table 4 summarized the results of the overall mass balance for the bio-oil reforming under three experimental conditions. Based on the estimation of the carbon balance, most of the carbon in the bio-oil was converted into CO_2 and CO, and the liquid products were minor in the case of high bio-oil's conversion. In the case of lower temperature and/or lower current, however, both carbon conversion and the hydrogen yield were low, and the cooled liquid contains a large amount of un-reacted bio-oil. It is very difficult to separate various liquid products from the un-reacted bio-oil,

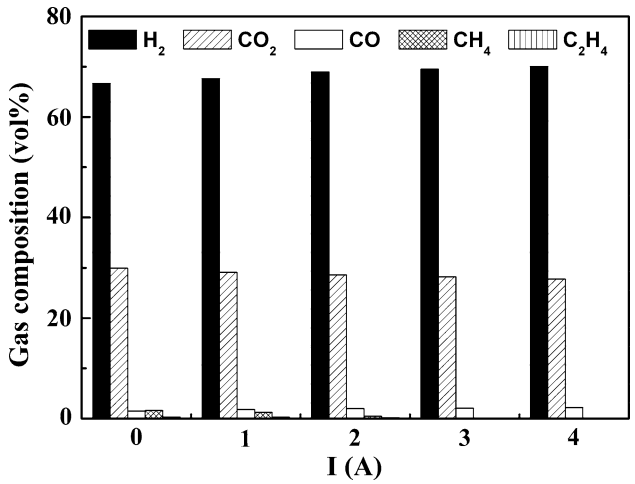

Fig. 3 Influence of the current on the gaseous product compositions of H_2, CO_2, CO, CH_4, and C_2H_4 over the NiCuZn–Al_2O_3 catalyst. Reforming conditions: $T = 450$ °C, $S/C = 6.3$, $GHSV = 5{,}200\ h^{-1}$, and $P = 1$ atm

Table 4 The mass balance of carbon for the bio-oil reforming under three experimental conditions

	Test-1[b]	Test-2[c]	Test-3[d]
% Carbon in gas phase effluent			
% Carbon in CO_2 product	52.7	76.8	90.9
% Carbon in CO product	2.6	5.1	6.9
% Carbon in CH_4 product	2.8	1.2	0.1
Coke	0.7	0.8	1.8
% Carbon in gas phase effluent:	33.3	11.8	–
Carbon balance(% feed)[a]	92.1	95.7	99.7

[a] The carbon balance defined as the ratio of all C-containing product moles to the consumed moles of the oxygenated organic compounds ($C_nH_mO_k$), accounting for stoichiometry

[b] The reforming conditions: $T = 450$ °C, $I = 0$ A, $S/C = 6.3$, $GHSV = 5{,}200\ h^{-1}$, and $P = 1$ atm

[c] The reforming conditions: $T = 450$ °C, $I = 2$ A, $S/C = 6.3$, $GHSV = 5{,}200\ h^{-1}$, and $P = 1$ atm

[d] The reforming conditions: $T = 450$ °C, $I = 4$ A, $S/C = 6.3$, $GHSV = 5{,}200\ h^{-1}$, and $P = 1$ atm

since the bio-oil contains a large number of complex compounds such as hydroxyaldehydes, hydroxyketones, sugars, carboxylic acids, phenolics, and so forth. To make clear the selectivity of products in ECR, we are studying the reforming of the model compounds (e.g., acetic acid, ethanol etc.).

The stability of the NiCuZn–Al_2O_3 catalyst during the bio-oil electrochemical catalytic reforming was tested by measuring the yield of hydrogen as a function of the time on stream. Figure 4 shows the typical curves for the yield of hydrogen measured at I = 2.9 A, T = 500 °C, S/C = 6.3, $GHSV$ = 5,200 h^{-1}. No obvious change of the hydrogen yield was observed for the initial 5 h. Slow decrease of the hydrogen yield was observed for the longer term observation, indicating a gradual deactivation of the catalyst during the bio-oil's electrochemical catalytic reforming. The hydrogen yield gradually decreases by about 10% (from about 90% to 80%) for 20 h reforming, and dropped to 50% of initial value for about 33 h reforming. The catalyst's deactivation, occurring in the process of the bio-oil's reforming, may mainly caused by the deposition of carbon (coke-formation) on the catalyst [39]. The amount of the carbon deposition estimated by the TGA measurements was about 10.6% after the bio-oil's electrochemical catalytic reforming for 33 h reforming at I = 2.9 A, T = 500 °C, S/C = 6.3, $GHSV$ = 5,200 h^{-1}.

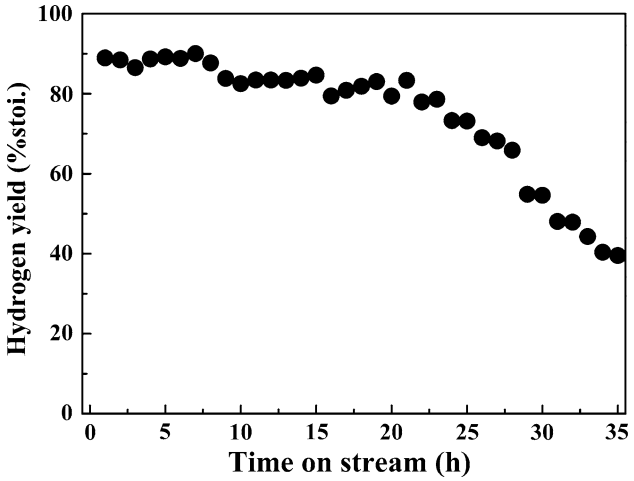

Fig. 4 Effect of time on stream on the hydrogen yield over the NiCuZn–Al_2O_3 catalyst. Reforming conditions: I = 2.9 A, T = 500 °C, S/C = 6.3, $GHSV$ = 5,200 h^{-1}, and P = 1 atm

The alterations of the atomic states on the catalyst's surfaces before and after the electrochemical catalytic reforming of bio-oil were investigated by the XPS measurements. Figure 5 shows the Ni/Cu/Zn XPS spectra of (a) the pristine NiCuZn–Al_2O_3 catalyst, (b) the used ones after the ECR of bio-oil, and (c) the treated catalyst via a current passing through the catalyst under the argon ambience, respectively. As can be seen from Figure 5(a), the bind energy at about 855.5 eV and 861.7 eV were observed for the pristine catalyst, which were assigned to the main line of $Ni^{2+}(2p_{3/2})$ and its satellite [32, 65], respectively. After the electrochemical catalytic reforming

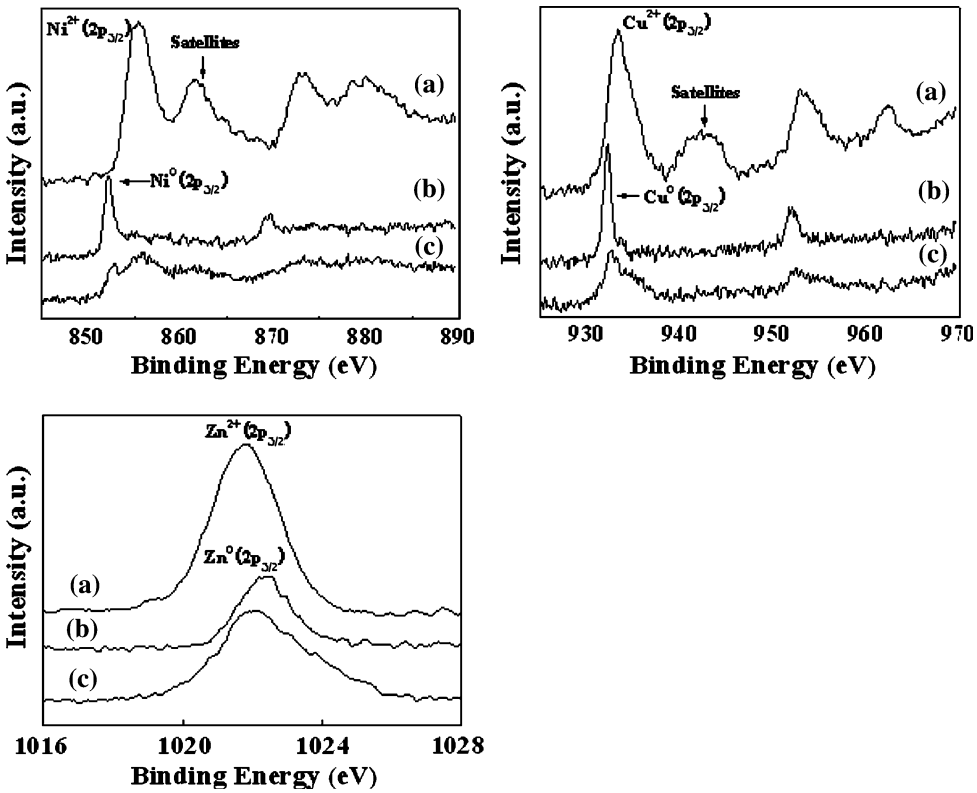

Fig. 5 Ni/Cu/Zn XPS spectra for **a** fresh NiCuZn–Al_2O_3 catalyst, **b** the used NiCuZn–Al_2O_3 catalyst after the electrochemical catalytic reforming for 33 h, reforming conditions: I = 2.9A, T = 500 °C, S/C = 6.3, $GHSV$ = 5,200 h^{-1}, and P = 1 atm, and **c** the treated NiCuZn–Al_2O_3 catalyst via a current passing though the catalyst under the argon ambience for 30 h (treatment conditions: I = 3.2A, T = 550 °C, $GHSV$ = 6,200 h^{-1}, and P(Ar) = 1 atm), respectively

of bio-oil, a new and strong peak near 852.6 eV was observed in the Ni XPS spectrum (Fig. 5b), corresponding to the peak of the metallic Ni^0 ($2p_{3/2}$) [32, 65]. The main line and its satellite of $Ni^{2+}(2p_{3/2})$ disappeared synchronously. The above results clearly showed that Ni was in +2 "formal" oxidation states in the fresh catalyst prepared and almost all of Ni^{2+} (i.e., the NiO phase) was reduced to metallic Ni^0 after the electrochemical catalytic reforming of bio-oil for 33 h. The reduction of Ni^{2+} would be mainly attributed to the surface reaction of the ionic state Ni^{2+} with the thermal electrons through $Ni^{2+} + 2e^- \rightarrow Ni^0$ together with the reduction by hydrogen formed in the reforming of bio-oil (i.e., $Ni^{2+} + H_2 \rightarrow Ni^0$). The reduction behavior from the oxidation state to the metallic phase was also observed when a current passed through the catalyst under the argon ambience (Fig. 5c). Figure 5 also displays the Cu XPS spectra (930–970 eV) and the Zn XPS spectra (1,016–1,028 eV) both from three samples mentioned above. The reduction from +2 "formal" oxidation states of $Cu^{2+}(2p_{3/2})$(933.4 eV) and $Zn^{2+}(2p_{3/2})$(1021.8 eV) into the metallic $Cu^0(2p_{3/2})$(932.5 eV) and $Zn^0(2p_{3/2})$(1022.4 eV) was also identified after the ECR of bio-oil or current-applied samples under the argon ambience.

Figure 6 (a–c) shows typical XRD spectra from the three samples mentioned above. For the fresh catalyst (Fig. 6a), the oxide states were observed. On the other hand, the XRD pattern for the used catalyst after ECR is quite different from that of the fresh one. As shown in Fig. 6(b), a series of new peaks appeared for the used ones after the ECR, corresponding to the metallic phases (i.e., Ni^0, Cu^0, and Zn^0). This means that the oxide states was reduced into the metallic states during the ECR process, which agreed with the XPS results. The reduction of the oxide states would be mainly attributed to the reactions of the ionic state M^{2+} with the thermal electrons through $M^{2+} + 2e^- \rightarrow M^0$ together with the reduction by hydrogen formed in the reforming of bio-oil (i.e., $M^{2+} + H_2 \rightarrow M^0$). This explanation was supported by two facts: (1) the desorption of the thermal electrons from the electrified catalyst was directly observed by the TOF measurements (Fig. 7) and (2) the reduction from the oxidation state to the metallic phase was also observed when a current passed through the catalyst under the argon or helium ambience (i.e., without reducing reagents such as H_2, (Figs. 5c and 6c). Electrons on a metal or a metal oxide surface, which play a role of reduction also occurred on the cathode of a *solid oxide fuel cell* (e.g., $O_2 + 4e^- \rightarrow 2O^{2-}$) [66, 67]. Moreover, the Cu sinter after the reforming under the investigated condition seems not to be serious since the clear XRD diffraction peaks of Cu at $2\theta = 43.3^o$, 50.4^o and 74.1^o was also clearly observed for the sample after the reforming.

To further investigate the dissociation and reforming in ECR, we tested using ethanol as a model of the oxygenated organic compounds for simplifying the reaction system under the low-pressure (10^{-1} Pa) conditions (Fig. 7a–d). The species desorbed from the catalyst surface were detected by an anionic time-of-flight (TOF) mass

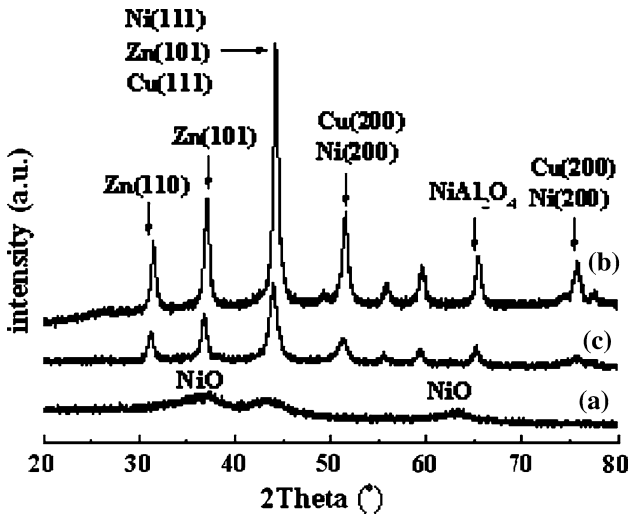

Fig. 6 XRD spectra for **a** fresh NiCuZn–Al_2O_3 catalyst, **b** the used NiCuZn–Al_2O_3 catalyst after ECR for 33 h, reforming conditions: $I = 2.9$A, $T = 500$ °C, $S/C = 6.3$, $GHSV = 5{,}200$ h^{-1}, and $P = 1$ atm, and **c** the treated NiCuZn–Al_2O_3 catalyst via a current passing though the catalyst under the argon ambience for 30 h (treatment conditions: $I = 3.2$A, $T = 550$ °C, $GHSV = 6{,}200$ h^{-1}, and P(Ar) = 1 atm)

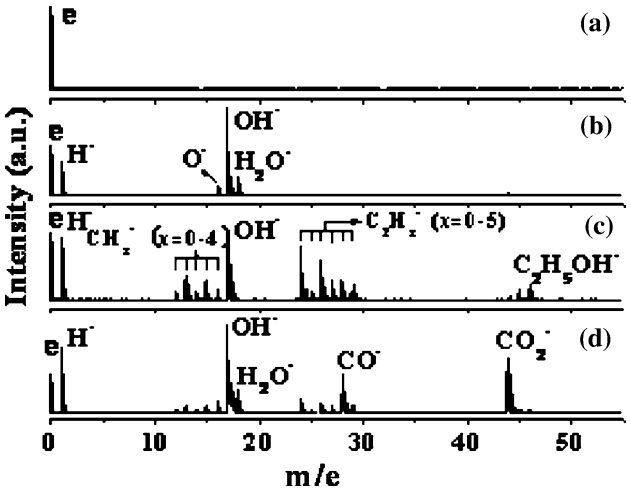

Fig. 7 Typical TOF spectra measured under following experimental conditions, including **a** the current passed through the catalyst in the argon ambience ($I = 3.0$ A, $T = 580$ °C, P(Ar) = 2.9×10^{-1} Pa), **b** the mixture of H_2O/Ar fed onto the electrified catalyst ($I = 2.9$ A, $T = 580$ °C, $P(H_2O) = 0.5 \times 10^{-1}$ Pa, P(Ar) = 2.3×10^{-1} Pa), **c** the mixture of C_2H_5OH/Ar fed onto the electrified catalyst ($I = 2.9$ A, $T = 580$ °C, $P(C_2H_5OH) = 0.5 \times 10^{-1}$ Pa, P(Ar) = 2.3×10^{-1} Pa), **d** the mixture of H_2O/C_2H_5OH/Ar fed onto the electrified catalyst ($I = 3.0$ A, $T = 580$ °C, $P(C_2H_5OH) = 0.4 \times 10^{-1}$ Pa, $P(H_2O) = 1.4 \times 10^{-1}$ Pa, P(Ar) = 1.0×10^{-1} Pa)

spectrometry. Without the current applied, no signal was observed from the catalyst surface. When the current passed through the catalyst in the argon ambience (Fig. 7a), only one peak near the mass numbers of zero was observed, corresponding to the thermal electrons desorbed from the electrified Ni–Cr wire and the catalyst surface. When water/argon were fed onto the electrified catalyst, three new peaks appeared, corresponding to $H^-(m/z = 1)$, $OH^-(m/z = 17)$, and $H_2O^-(m/z = 18)$, respectively (Fig. 7b). These anionic fragments would form by the dissociation of water with the thermal electrons on the catalyst surface (e.g., $e^-(s) + H_2O(s) \rightarrow OH^-(s) + H(s)$, where "s" represents the surface). The formation of OH^- was also observed on the anionic surface storage-emission materials of $[Ca_{24}Al_{28}O_{64}]^{4+}\cdot(OH^-)_4$ surface when H_2O and electrons was fed on the material [63]. When the mixture of C_2H_5OH/Ar was fed onto the electrified catalyst, a series of new peaks of H^-, OH^-, $CH_x^-(x = 0–4)$, $C_2H_x^-(x = 0–5)$, $C_2H_5OH^-$ appeared (Fig. 7c). The hydrocarbon fragments would form via the dissociation of ethanol caused by the thermal electrons on the surface (i.e., $e^-(s) + C_2H_5OH(s) \rightarrow C_xH_y^-(s) + \ldots$, where s represents the surface). As the mixture of H_2O/C_2H_5OH/Ar was injected onto the electrified catalyst, the peak of CO_2^- was observed (Fig. 7d), indicating that the reforming reaction of ethanol (i.e., $C_2H_5OH(s) + H_2O(s) \rightarrow CO_2(s) + H_2(s)$) occurred. The above results further confirmed that the thermal electrons play an important role in promoting the decomposition and reforming of the oxygenated organic compounds.

Present results show that the current applied to the catalyst significantly promotes the bio-oil's reforming and the catalyst reduction, which will be discussed as follows. First, both the ECR mode (i.e., inner heating) and the CSR mode (i.e., outside heating) had temperature distribution in the catalyst bed. The maximal temperature gradients in ECR were higher than those in CSR (Table 3). It was noticed that high carbon conversion (>90%) were obtained via the ECR mode at near 400 °C (the averaged temperature) with a current over 3.0 A (Fig. 2). To obtain such carbon-conversion, temperature near 600 °C is required if we use the CSR mode over the catalyst by the outside heating. However, the maximal temperature gradient in ECR was about 18 °C when the average temperature in the bed was near 400 °C. The temperature in the center of the catalyst bed, generally, is approximately close to the average temperature (Table 3) in our investigated range. Accordingly, the effects of the current on the production of hydrogen from bio-oil in ECR mode cannot be simply attributed to the effect of the temperature gradient in our investigated range, based on the results of the temperature distribution. In addition, the reduction behavior of Ni^{2+}/Cu^{2+}/Zn^{2+} into the metallic Ni^0/Cu^0/Zn^0 phases via a current passing through the catalyst without adding any reducing agents (Figs. 5c and 6c) cannot be explained by the effect of the temperature gradient.

The second probable explanation for the effect of current on the bio-oil reforming may cause by an additional reduction of the oxide states into the metallic states during the ECR process. In order to investigate the difference between the oxide catalyst and the metallic state' catalyst, we have compared the reforming performance over the $NiO–Al_2O_3$ and $Ni–Al_2O_3$ catalysts respectively. As shown in Fig. 8, both the $NiO–Al_2O_3$ and $Ni–Al_2O_3$ catalysts have the catalytic activity for the bio-oil's reforming. The reforming activity over the $Ni–Al_2O_3$ catalyst is somewhat higher than that over the $NiO–Al_2O_3$ catalyst in our investigated region. In particular, the prominent influence of the current on the carbon conversion was also observed for the metallic state' $Ni–Al_2O_3$ catalyst (Fig. 8d). This means that the promoting effects of the current on the production of hydrogen from bio-oil observed in the ECR process via the $NiO/CuO/ZnO–Al_2O_3$ catalyst could not be completely attributed to the catalyst reduction. Moreover,

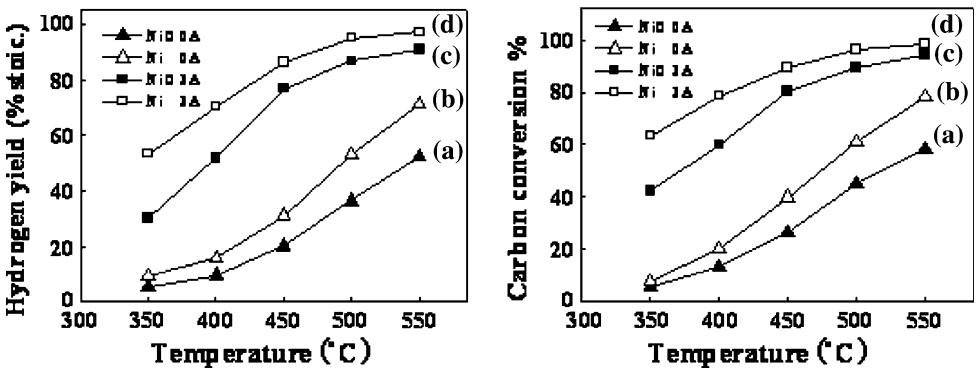

Fig. 8 The yield of hydrogen (left) and the carbon conversion (right), measured as a function of temperature for **a** CSR ($I = 0$ A) using the $NiO–Al_2O_3$ catalyst, **b** CSR ($I = 0$ A) using the $Ni–Al_2O_3$ catalyst, **c** ECR ($I = 3.0$ A) using the $NiO–Al_2O_3$ catalyst, **d** ECR (I = 3.0 A) using the $Ni–Al_2O_3$ catalyst, respectively. Other reforming conditions were fixed at $T = 350$, 400, 450, 500, 550 °C respectively, $S/C = 5.8$, $GHSV = 6{,}048\ h^{-1}$, and $P = 1$ atm

the contribution to the bio-oil's reforming from the Ni–Cr wire is minor (not shown here). When we compared the performance between ECR and CSR, all experiments were carried out in the reactor installed the Ni–Cr wire. Thus, the effects of the current on the bio-oil reforming can not be attributed to the additional activity due to the Ni–Cr wire.

Third, the promoting effects of current would be explained by the enhancement of the decomposition and reforming of the oxygenated organic compounds in the bio-oil during ECR via thermal electrons. It is well known that when an electrified metal or a metal oxide is heated, electrons can boil off its surface, leading to thermal emission of electrons from surface (i.e., thermal electron emission) [68]. The thermal electron emission has been widely used for vacuum parts, e.g., thermal cathode ionization vacuometer, vacuum tube and electron-beam sources [69–71]. It has been reported that thermal electrons on a metal or a metal oxide surface play an important role in the reduction process (e.g., $O_2 + 4e^- \rightarrow 2O^{2-}$ occurring on the cathode of a *solid oxide fuel cell)* [66, 67], and in the molecular decomposition or ionization processes [62, 63]. The thermal electrons from the electrified Ni–Cr wire in the ECR mode is one of the most likely candidates to explain the promoting effect of the bio-oil's decomposition, its reforming and the reduction of the catalyst. This proposal is supported by the following observation. (1) The presence of the thermal electrons both on the electrified Ni–Cr wire and on the electrified catalyst surface was directly demonstrated by the TOF measurements (Fig. 7a). (2) The dissociation of water into OH^- (Figure 7b) and the ethanol dissociation into the anionic hydrocarbon fragments (Fig. 7c) by the thermal electrons on the electrified catalyst surface were also observed (i.e., $e^-(s) + C_2H_5OH(s) \rightarrow CH_x^-(s) + \ldots$, and $e^-(s) + H_2O(s) \rightarrow OH^-(s) + H(s)$, where "s" represents the surface.). (3) A part or complete reduction from the oxidation states to the metallic states in the NiO/CuO/ZnO/Al_2O_3 catalyst was observed when a current passed through the catalyst under the argon or helium ambience (Figs. 5c and 6c), being attributed to the reaction of Ni^{2+} with the thermal electrons (i.e., $Ni^{2+} + 2e^- \rightarrow Ni^0$). Accordingly, the thermal electrons may play an important role in promoting the decomposition, reforming of bio-oil and the catalyst reduction, leading to the increase of the carbon conversion and the hydrogen yield in the ECR process. Further work is also required to make clear the decomposition and reforming mechanism. Work toward this goal is in progress.

4 Conclusion

In summary, we present a new and effective method for production of hydrogen via the electrochemical catalytic reforming of the bio-oil over the NiCuZn–Al_2O_3 reforming catalyst, giving well reforming performance including high hydrogen-yield and high carbon-conversion even at low reforming temperature (300–400 °C). Based on the analyses of TOF, XPS and XRD, the thermal electrons would play important roles in the dissociation of the oxygenated organic compounds in the bio-oil, the catalyst reduction and production of hydrogen during the bio-oil electrochemical catalytic reforming.

Acknowledgements The authors are grateful to the support of the "National Basic Research Program" (973 Program No. 2007CB210206) of Ministry of Science and Technology of China, the "National High Tech Research and Development Program" (863 Program No. 2006AA05Z118) and the General Program of the National Natural Science Foundation of China (No. 50772107) and Demonstration and Applied Investigation of Biomass Clean Energy Base (No. 2007-15).

References

1. Prakash D, Vaidya , Alirio E, Rodrigues (2006) Chem Eng J 117:39
2. Haryanto A, Fernando S, Murali N, Adhikari S (2005) Energy Fuels 19:2098
3. Das D, Veziroglu TN (2001) Int J Hydrogen Energy 26:13
4. Chen ZX, Yan YB, Elnashaie SSEH (2004) Chem Eng Sci 59:1965
5. Huber GW, Shabaker JW, Dumesic JA (2003) Science 300:2075
6. Chornet E, Czernik S (2002) Nature 418:928
7. Cortright RD, Davda RR, Dumesic JA (2002) Nature 418:964
8. Li WZ, Yan YJ, Li TC, Ren ZW, Huang M, Wang J, Chen MQ, Tan ZC (2008) Energy Fuels 22:1233
9. Nishikawa J, Nakamura K, Asadullah M, Miyazawa T, Kunimori K, Tomishige K (2008) Catal Today 131:146
10. Huber GW, Iborra S, Corma A (2006) Chem Rev 106:4044
11. Corella J, Toledo JM, Molina G (2007) Ind Eng Chem Res 46:6831
12. Czernik S, Bridgwater AV (2004) Energy Fuels 18:590
13. Zhu XF, Zheng JL, Guo QX, Zhu QS (2006) J Environ Sci 18:392
14. Zhu XF, Venderbosch R (2005) Fuel 84:1007
15. Zheng JL, Zhu XF, Guo QX, Zhu QS (2006) Waste Manag 26:1430
16. Zhu XF (2001) China Patent 00241135.0
17. Zhu XF (2002) China Patent 01263584.7
18. Ba T, Chaala A, Garcia-Perez M, Rodrigue D, Roy C (2004) Energy Fuels 18:704
19. Corma A, Iborra S, Velty A (2007) Chem Rev 107:2411
20. Rioche C, Kulkarni S, Meunier FC, Breen JP, Burch R (2005) Appl Catal B 61:130
21. Trimm DL (1997) Catal Today 37:233
22. Fatsikostas AN, Verykios XE (2004) J Catal 225:439
23. Armor JN (1999) Appl Catal A 176:159
24. Nurunnabi M, Fujimoto K, Suzuki K, Li BT, Kado S, Kunimori K, Tomishige K (2006) Catal Commun 7:73
25. Wang D, Czernik S, Montane′ D, Mann M, Chornet E (1997) Ind Eng Chem Res 36:1507
26. Garcia L, French R, Czernik S, Chornet E (2000) Appl Catal A 201:225
27. Fierro V, Akdim O, Mirodatos C (2003) Green Chem 5:20
28. Fierro V, Klouz V, Akdim O, Mirodatos C (2002) Catal Today 75:141

29. Marino F, Boveri M, Baronetti G, Laborde M (2004) Int J Hydrogen Energy 29:67
30. Marino F, Boveri M, Baronetti G, Laborde M (2001) Int J Hydrogen Energy 26:665
31. Velu S, Satoh N, Gopinath CS, Suzuki K (2002) Catal Lett 82(1–2):145
32. Velu S, Suzuki K, Vijayaraj M, Barman S, Gopinath CS (2005) Appl Catal B 55:287
33. Klouz V, Fierro V, Denton P, Katz H, Lisse JP, Bouvot-Mauduit S, Mirodatos C (2002) J Power Sour 105:26
34. Davidian T, Guilhaume N, Iojoiu E, Provendier H, Mirodatos C (2007) Appl Catal B 73:116
35. Czernik S, Evans R, French R (2007) Catal Today 129:265
36. Marquevich M, Czernik S, Chornet E, Montane D (1999) Energy Fuels 13:1160
37. Wang D, Czernik S, Chornet E (1998) Energy Fuels 12:19
38. Rioche C, Kulkarni S, Meunier FC, Breen JP, Burch R (2005) Appl Catal B Environ 61:144
39. Wang ZX, Pan Y, Dong T, Zhu XF, Kan T, Yuan LX, Torimoto Y, Sadakata M, Li QX (2007) Appl Catal A 320:24
40. Wang ZX, Dong T, Yuan LX, Kan T, Zhu XF, Torimoto Y, Sadakata M, Li QX (2007) Energy Fuels 21:2421
41. Li QX, Yuan LX, Chen YQ, Kan T, Qiu SB, Sadakata M (2008) China Patent 101177239A
42. Dong T, Wang ZX, Yuan LX, Torimoto Y, Sadakata M, Li QX (2007) Catal Lett 119:29
43. Fatsikostas AN, Kondarides DI, Verykios XE (2001) Chem Commun 851
44. Goula MA, Kontou SK, Tsiakaras PE (2004) Appl Catal B 49:135
45. Torres JA, Llorca J, Casanovas A, Domınguez M, Salvado J, Montane D (2007) J Power Sour 169:158
46. Kechagiopoulos PN, Voutetakis SS, Lemonidou AA, Vasalos IA (2006) Energy Fuels 20:2155
47. Jacobs G, Keogh RA, Davis BH (2007) J Catal 245:326
48. Basagiannis AC, Verykios XE (2007) Int J Hydrogen Energy 32:3343
49. Galdamez JR, Garcia L, Bilbao R (2005) Energy Fuels 19:1133
50. Takanabe K, Aika K, Seshan K, Lefferts L (2004) J Catal 227:101
51. Takanabe K, Aika K, Inazu K, Baba T, Seshan K, Lefferts L (2006) J Catal 243:263
52. Takanabe K, Aika K, Seshan K, Lefferts L (2006) Chem Eng J 120:133
53. Basagiannis AC, Verykios XE (2007) Catal Today 127:256
54. Bimbela F, Oliva M, Ruiz J, Garcia L, Arauzo J (2007) J Anal Appl Pyrolysis 79:112
55. Davidian T, Guilhaume N, Daniel C, Mirodatos C (2008) Appl Catal A 335:64
56. Vagia EC, Lemonidou AA (2007) Int J Hydrogen Energy 32:212
57. Kechagiopoulos PN, Voutetakis SS, Lemonidou AA, Vasalos IA (2007) Catal Today 127:246
58. Liguras DK, Kondarides DI, Verykios XE (2003) Appl Catal B 43:345
59. Aupretre F, Descorme C, Duprez D (2002) Catal Commun 3:263
60. Kugai J, Velu S, Song C (2005) Catal Lett 101:255
61. Domine ME, Iojoiu EE, Davidian T, Guilhaume N, Mirodatos C (2008) Catal Today 133–135:565
62. Huang F, Li J, Wang L, Dong T, Tu J, Torimoto Y, Sadakata M, Li QX (2005) J Phys Chem B 109:12032
63. Li J, Huang F, Wang L, Wang ZX, Yu SQ, Torimoto Y, Sadakata M, Li QX (2005) J Phys Chem B 109:14599
64. Li QX, Hosono H, Hirano M, Hayashi K, Nishioka M, Kashiwagi H, Torimoto Y, Sadakata M (2003) Surf Sci 527:100
65. Srinivas D, Satyanarayana CVV, Potdar HS, Ratnasamy P (2003) Appl Catal A 246:323
66. Ricoult MB (2008) Sol Stat Sci 10:670
67. Tsipis EV, Kharton VV (2008) J Sol Stat Electrochem 12:1367
68. Somorjai GA (1994) Introduction to surface chemistry and catalysis. Wiley-Interscience, New York
69. Shiozawa K, Neo Y, Okada M, Matsumoto T, Takahashi M, Hashiguchi G, Mimura H (2007) J Vac Sci Technol B 25:666
70. Singleton JH (2001) J Vac Sci Technol A 19:1712
71. Christov SG (1966) Phys Stat Sol 17:11